Detection performance of trigger-controlled Geiger-mode avalanche photodiodes in weak optical signal detection

Peng Zhao (赵 鹏)[1,2,*], Yabo Yuan (袁亚博)[1,2], Yan Zhang (张 艳)[1,2], and Weiping Qian (钱卫平)[2]

[1]*Beijing Institute of Tracking and Telecommunications Technology, Beijing 100094, China*
[2]*Key Laboratory of Space Object Measurement, Beijing 100094, China*
**Corresponding author: roczhao1991@163.com*

Received November 17, 2015; accepted January 25, 2016; posted online April 1, 2016

This Letter introduces a trigger-controlled Geiger-mode avalanche photodiode (GM-APD). A hierarchical look-back-upon tree recurrence method is given to predict the performance of trigger-controlled GM-APDs under different trigger-count upper limits. In addition, the normalized detection probability is defined to evaluate the detection performance of trigger-controlled GM-APDs in typical weak optical signal detection (impulse noise and continuous noise situations). Theoretical analyses show that the trigger-controlled GM-APD improves the detection performance of GM-APDs in weak optical signal detection via the optimization of the trigger-count upper limit, compared with single-trigger and multi-trigger GM-APDs.

OCIS codes: 280.3420, 040.1345, 280.4788.
doi: 10.3788/COL201614.042801.

Geiger-mode avalanche photodiodes (GM-APDs) possess high sensitivity and high gain to detect a single photon[1]. However, the traditional gated GM-APD with a long dead time can only trigger once in one gate; hence, it is called the single-trigger GM-APD. Once the detector is triggered, the signal cannot be triggered during the rest of the gate. Thus, the detection probability of signals arriving afterward will be reduced, especially in weak optical signal detection[2]. Typical weak optical signal detection scenarios can generally be divided into impulse noise and continuous noise situations.

In impulse noise situations, the signal arrives after a high noise pulse, which can be found using optical time-domain reflectometry[3] and partially obscured target laser ranging[4]. In continuous noise situations, the weak signal is obscured by the continuous strong noise, which can be found in faithful swapping experiments[5] and diffuse reflection laser ranging (DRLR)[6].

Johnson *et al.*[7] first proposed the multi-trigger GM-APD to improve the detection performance for partially obscured target detection in laser ranging, in which a GM-APD with a short dead time can be triggered multiple times in one gate as long as the dead time is over. Furthermore, Oh *et al.*[3,8] experimentally verified the effectiveness of the multi-trigger GM-APD for partially obscured target detection, compared with the single-trigger GM-APD. However, their investigations were limited to partially obscured target laser ranging. Moreover, the multi-trigger GM-APD was not well designed for weak optical signal detection, since the trigger count of the multi-trigger GM-APD only takes the maximum during the gate.

In this Letter, the trigger-controlled GM-APD is introduced to improve the GM-APD performance in weak optical signal detection. First, the hierarchical look-back-upon tree recurrence (H-LTR) method is given to predict the performance of trigger-controlled GM-APDs under different trigger-count upper limits. Based on the theoretical performance prediction, the normalized detection probability is defined to evaluate the detection performance in impulse noise and continuous noise situations. Theoretical analyses show that the trigger-controlled GM-APD improves the detection performance of GM-APDs in weak optical signal detection via the optimization of the trigger-count upper limit, making a solid foundation for a hardware implementation.

For GM-APDs, each trigger depends on the generation of primary electrons (PEs) and that the avalanche is followed in sequence[9]. PEs are generated mainly from the light absorbed by imperfect quantum efficiency as well as the dark noise inside[10] the GM-APD. The absorbed light includes echo light reflected from the target and background light. In general, the echo light is assumed to be a function of time, while the background light is not. Thus, the optical power of the echo light and background light are defined as $P_e(t)$ and P_b, respectively. In addition, the count rate of the dark noise is defined as R_d, and the probability that a PE will trigger an avalanche is incorporated into the imperfect quantum efficiency, η_{qe}. Then, the input rate, $\psi(t)$, is written as

$$\psi(t) = \eta_{\mathrm{qe}}(P_e(t) + P_b)/h\nu + R_d, \tag{1}$$

where h is Planck's constant, v is the laser's optical frequency, and the product hv is the photon energy.

However, once the avalanche occurs, a period of dead time, T_d, follows, in which the GM-APD is blocked and unavailable for re-triggering. The GM-APD will not be triggered again unless the dead time has ended and the gating time, T_g, has not. Therefore, the dead time and

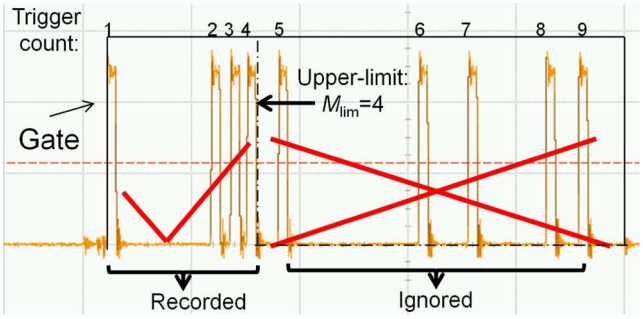

Fig. 1. Example of the trigger-controlled GM-APD's operating scheme.

the gating time together decide the maximum trigger count, $M_{\max}$, of the GM-APD:

$$M_{\max} = \frac{T_g}{T_d}. \tag{2}$$

Regardless of the value of $M_{\max}$, the trigger count of the single-trigger GM-APD is limited to one during the gate. Alternatively, the multi-trigger GM-APD increases the trigger count to $M_{\max}$ to improve the detection performance. However, neither the single-trigger GM-APD nor the multi-trigger GM-APD can take arbitrary trigger counts between one and the maximum. In this Letter, we introduce the concept of a trigger-controlled GM-APD where the upper limit of the trigger count, denoted as $M_{\lim}$, can be controlled to vary from one to $M_{\max}$. An example of the trigger-controlled GM-APD's operating scheme is shown in Fig. 1.

As shown in Fig. 1, if the trigger count reaches its upper limit during the gate, the trigger-controlled GM-APD will close and all subsequent trigger pulses will be ignored. Meanwhile, if the trigger count is less than $M_{\lim}$ during the gate, all trigger-pulse arrival times will be recorded and the trigger-controlled GM-APD will close at the end of the gate. In addition, the single-trigger GM-APD can only trigger once in the gate and the multi-trigger GM-APD will remained armed during the whole gate. In this Letter, we focus on the theoretical performance prediction and analysis of the trigger-controlled GM-APD, compared with the single-trigger GM-APD and the multi-trigger GM-APD.

The count rate is generally used to reflect the performance of the detector. In practice, the time-dependent distribution of the GM-APD output rate is obtained via the accumulation of detected trigger-pulse arrival times during the gate. In the performance prediction theory, the distribution could be predicted based on a priori knowledge of the detector and the system without any practical testing. The LTR method currently possesses a better calculation performance than other performance prediction methods for multi-trigger GM-APDs among all ranges of dead time and input diversity[11]. However, it can only predict the output rate of multi-trigger GM-APDs. Hereafter, the H-LTR method is used to predict the output rate under different upper limits of the trigger count.

We define $\xi_p(t, M)$ as the partial output rate for trigger count M, and $\xi(t, M_{\lim})$ as the output rate when the upper limit is $M_{\lim}$. The output rate is obtained by summing the partial output rates for trigger counts less than $M_{\lim}$. Thus, $\xi(t, M_{\lim})$ is obtained by

$$\xi(t, M_{\lim}) = \sum_{M=1}^{M_{\lim}} \xi_p(t, M), \times 0 \le t \le T_g, 1 \le M \le M_{\lim} \le M_{\max}. \tag{3}$$

In the discrete-time condition, the gate time, T_g, is discretized into N bins with the same time period T_b, where N is equal to ceil(T_g/T_b) and ceil() is the ceiling function. Meanwhile, the dead time, T_d, is discretized into d bins, where d is equal to ceil(T_d/T_b). Then, the mean number of PEs generated from $\psi(t)$ at the ith bin, $\overline{K}_i$, is given by

$$\overline{K}_i = \int_{(i-1)T_b}^{iT_b} \psi(t)\mathrm{d}t. \tag{4}$$

Since the number of PEs is generally assumed to follow the Poisson distribution, the probability that at least one PE is generated at the ith bin is given by[9,12]

$$P_{\mathrm{PE}}(i) = 1 - \exp(-\overline{K}_i). \tag{5}$$

We define $P_a(i, M)$ as the probability of an avalanche at the ith time interval for trigger count M. Because the GM-APD avalanche only occurs once, no matter how many PEs are generated at the ith bin, the probability of an avalanche is equal to the average number of avalanches at the ith time bin. Then, $\xi_p(t, M)$ can be obtained by

$$\xi_p(t, M) = P_a(i, M)/T_b, \times (i-1)T_b \le t \le iT_b, 1 \le M \le M_{\max}. \tag{6}$$

Define states '1', '0', and 'X' as the states where the GM-APD succeeds in avalanching because of the PE generation, fails in avalanching because no PEs exist, and is blocked during the dead time, respectively. In order to calculate $P_a(i, M)$ for different M, the look-back-upon rules[11] in the LTR method should be modified to consider the trigger count M as follows:

a) The initial state is '1' at the ith bin;

b) the prior states of '0' or '1' are '0' and 'X';

c) the prior state of 'X' is '1' or 'X', depending on the location of the current state 'X' in the sequence of $\underbrace{1\leftarrow \mathrm{X}\cdots\mathrm{X}\leftarrow\mathrm{X}}_{d}$.

d) The number of trigger counts, M, increases by one once state '1' occurs,

where rule d) is newly added to introduce M. According to the modified look-back-upon rules, the hierarchical look-back-upon tree structure, defined as LT_i, is given. According to the rule a), LT_1 is defined as the single state '1' of the ith bin. According to rules b) and c), LT_1 could expand to LT_i after i times look-back-upon. At the jth look-back-upon $(1 < j \le i)$, possible states of the $i-j+1$th bin will be added next to the end of LT_{j-1}, and then LT_{j-1} expands to LT_j. According to rule d), newly added state '1' will located in the lower level, where a lower level means a bigger M. An example of

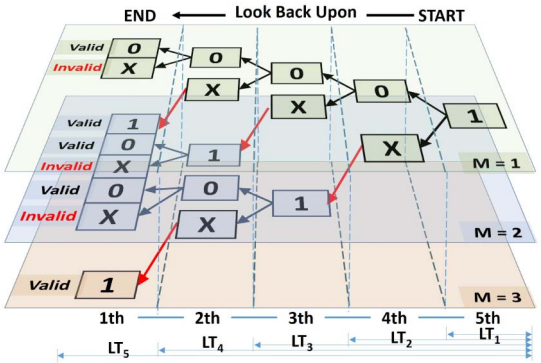

Fig. 2. Deduction of LT_5 when $i=5$ and $d=2$.

the deduction of LT_5 when the avalanche occurs at the fifth bin and $d=2$ is shown in Fig. 2.

States connected from the start to the end in the direction opposite the time sequence, denoted as a state connection, represent a possible case in a real situation. State connections ending with state 'X' are invalid because state 'X' cannot occur at the beginning of the gate time. Meanwhile, state connections ending with state '1' and state '0' are valid connections. Therefore, $P_a(i,M)$ can be calculated by summing the probabilities of all valid connections ending in the Mth level of LT_i. Because $d-1$ states that 'X' always follows once state '1' occurs in a state connection, the probability of a state connection is the product of the probabilities of all states '1' and '0' in the state connection.

According to the definitions of states '1' and '0', the probability of state '1' occurring at the ith bin is $P_{\rm PE}(i)$, and the probability of state '0' occurring at the ith bin is $1-P_{\rm PE}(i)$. Define $P_a^1(j,M)$ and $P_a^0(j,M)$ as the corresponding probabilities of valid connections in LT_j ending with state '1' and state '0' for the trigger count M, respectively. When LT_{j-1} expands to LT_j, the state '0' at the end of LT_j is added next to the state '0' or '1' at the end of LT_{j-1} in the same level. Therefore, $P_a^0(j,M)$ is obtained from $P_a^0(j-1,M)$ and $P_a^1(j-1,M)$ as Eq. (7):

$$\begin{cases} P_a^0(j,M)=0 & j=1,1\le M\le M_{\max} \\ P_a^0(j,M)=(1-P_{\rm PE}(i-j+1))\cdot & \\ (P_a^0(j-1,M)+P_a^1(j-1,M)) & 1<j\le i,1\le M\le M_{\max} \end{cases}, \quad (7)$$

where $P_a^0(1,M)$, $1\le M\le M_{\max}$, is equal to zero because LT_1 is a single state '1' of the ith bin.

The sequence, 1←X$\cdots$X←X, whose state '1' is located at the end of LT_j in the lower level, is added next to the state '0' or '1' at the end of LT_{j-d} in the higher level. Therefore, $P_a^1(j,M)$ is obtained from $P_a^0(j-d,M-1)$ and $P_a^1(j-d,M-1)$ as Eq. (8). Because only the single state '1' of LT_1 will exist in the first d LTs (LT_1-LT_d), the initial value of $P_a^1(j,M)$ is also shown in Eq. (8):

$$\begin{cases} P_a^1(j,M)=P_{\rm PE}(j) & j=1,M=1 \\ P_a^1(j,M)=0 & j=1,1<M\le M_{\max} \\ P_a^1(j,M)=0 & 1<j\le i,M=1 \\ P_a^1(j,M)=0 & 1<j\le d,1<M\le M_{\max} \\ P_a^1(j,M)=P_{\rm PE}(i-j+1)\cdot & \\ (P_a^0(j-d,M-1)+P_a^1(j-d,M-1)) & d<j\le i,1<M\le M_{\max} \end{cases}. \quad (8)$$

Then, $P_a^1(i,M)$ and $P_a^0(i,M)$ can be obtained according to Eqs. (7) and (8), and $P_a(i,M)$ is given by

$$P_a(i,M)=P_a^1(i,M)+P_a^0(i,M). \quad (9)$$

Thus, $\xi(t,M_{\rm lim})$ can be further obtained according to Eqs. (3) and (6). Based on the calculation of $\xi(t,M_{\rm lim})$, the normalized signal detection probability under different $M_{\rm lim}$, defined as $P_d(M_{\rm lim})$, is further proposed to evaluate the detection performance of the trigger-controlled GM-APD. $P_d(M_{\rm lim})$ is given by

$$P_d(M_{\rm lim})=\frac{\int_{T_{\rm ae}}^{T_{\rm ae}+T_p}\xi(t,M_{\rm lim}){\rm d}t}{\int_0^{T_g}\xi(t,M_{\rm lim}){\rm d}t}, \quad (10)$$

where T_p is the width of the echo light and $T_{\rm ae}$ is the arrival time of the echo light. A bigger P_d means more signal counts from the echo light are detected; these photos can be easily extracted from the fake counts. Meanwhile, a smaller $M_{\rm lim}$ means fewer counts (less data) are detected and the data processing cost decreases. Therefore, a bigger P_d is expected to be obtained with a smaller $M_{\rm lim}$.

For the impulse noise and continuous noise situations, input rates of noises have different forms. In the impulse noise situation, the signal arrives after a high noise pulse. The arrival time of the impulse noise is defined as $T_{\rm ai}$, and the width of the impulse noise is assumed to be the same as T_p. Then, the signal-to-noise ratio (SNR) in the impulse noise situation can be defined as

$${\rm SNR}_i=\frac{\int_{T_{\rm ai}}^{T_{\rm ai}+T_p}\psi(t){\rm d}t}{\int_{T_{\rm ae}}^{T_{\rm ae}+T_p}\psi(t){\rm d}t}. \quad (11)$$

In the continuous noise situation, the weak echo signal is obscured by a continuously strong noise. The strong noise is assumed to be distributed uniformly within the gate. Then, the SNR in the continuous noise situation can be defined as

$${\rm SNR}_c=\frac{\int_{T_{\rm ae}}^{T_{\rm ae}+T_p}\psi(t){\rm d}t}{\int_0^{T_g}\psi(t){\rm d}t-\int_{T_{\rm ae}}^{T_{\rm ae}+T_p}\psi(t){\rm d}t}. \quad (12)$$

In theoretical analyses, for the sake of simplicity, the arrival time of the echo light, $T_{\rm ae}$, is assumed to be centered at the middle of the gate, and the arrival time of the impulse noise, $T_{\rm ai}$, is 100 ns earlier. The echo light and the impulse noise are assumed to be rectangular where T_p is equal to 10 ns. Moreover, the dead time is 100 ns, the gating time is 1 μs, and the number of time bins is 1000.

Assume the echo light is at the single-photon level. Consequently, the total number of PEs generated from the echo light during the gate is assumed to be one on average. According to Eq. (10), $P_d(M_{\rm lim})$ under different $\rm SNR_i$ assumptions in the impulse noise situation is shown in Fig. 3(a), and $P_d(M_{\rm lim})$ under different $\rm SNR_c$ assumptions in the continuous noise situation is shown in Fig. 3(b).

As shown in Fig. 3(a), the normalized detection probability, P_d, increases when $M_{\rm lim}$ increases, while P_d remains almost unchanged when $M_{\rm lim}$ is greater than two. On the one hand, the maximum P_d of the trigger-controlled GM-APD is bigger than the single-trigger GM-APD ($M_{\rm lim}=1$). On the other hand, the detection performance of the trigger-controlled GM-APD is equal to that of the multi-trigger GM-APD ($M_{\rm lim}=M_{\rm max}$), whereas bigger trigger counts only bring a bigger data-processing cost to the entire system. Therefore, to obtain the best detection performance, the trigger-count upper limit of the trigger-controlled GM-APD should be optimized to the first two triggers ($M_{\rm lim}=2$). Moreover, the changing features of $P_d(M_{\rm lim})$ under different $\rm SNR_i$ assumptions are similar.

As shown in Fig. 3(b), P_d decreases when $\rm SNR_c$ decreases from 1:1 to 1:8. For a high $\rm SNR_c$, P_d reaches the maximum when the trigger count is only one. However, for a small $\rm SNR_c$, the peaks of the curves move to the right, and P_d reaches the maximum at bigger trigger counts. That is to say, the maximum P_d of the trigger-controlled GM-APD is bigger than the P_d of the single-trigger GM-APD ($M_{\rm lim}=1$) for a low $\rm SNR_c$. Meanwhile, the maximum P_d of the trigger-controlled GM-APD with fewer trigger counts is always bigger than the P_d of the multi-trigger GM-APD ($M_{\rm lim}=M_{\rm max}$).

Therefore, optimizing the trigger-count upper limit of the trigger-controlled GM-APD is a feasible way to obtain the best detection performance with less data, compared with single-trigger and multi-trigger GM-APDs in the impulse noise and the continuous noise situations, especially when the $\rm SNR_c$ is low.

To have an explicit understanding of the benefits, a simple simulation of a DRLR system using the trigger-controlled GM-APD in the continuous noise situation is given by Monte Carlo method. Here, we focus on the operating scheme of the trigger-controlled GM-APD, where complicated factors, such as atmosphere turbulence, are ignored. The time of flight (TOF) of the signals is recorded only when their trigger-count numbers are less than $M_{\rm lim}$. Then, the range residuals[13] under different $M_{\rm lim}$ are calculated based on the TOF. The range residual of the target is assumed to have a linear distribution. The repetition rate of the laser is 10 Hz and the $\rm SNR_c$ is 1:8. Other parameters and assumptions are equal to that of the continuous noise situation in the theoretical analyses. The range residuals under different $M_{\rm lim}$ after 60 s of observation of the DRLR simulation system are shown in Fig. 4.

In Fig. 4(a), which is the case of the single-trigger GM-APD, the trace of the target is hard to be detected. In Fig. 4(b), the trace of the target is just enough to be distinguished when $M_{\rm lim}$ is equal to 2. In Fig. 4(c), the trace of the target becomes very clear when $M_{\rm lim}$ is equal to 4. In Fig. 4(d), the trace of the target is almost as clear as Fig. 4(c), while the fake counts caused by the noise increase, since more trigger counts will be recorded. Additionally, Fig. 4(d) corresponds to the case of the multi-trigger GM-APD. Thus, through the optimization of the upper limit of trigger counts, trigger-controlled GM-APDs can achieve a better detection performance

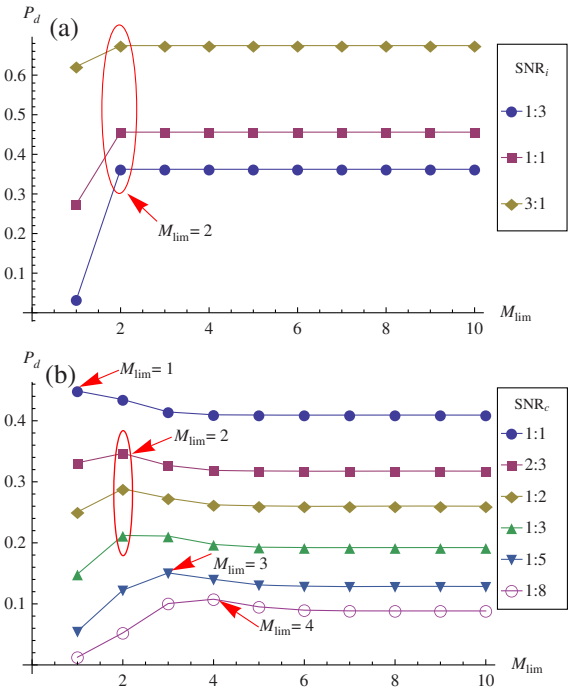

Fig. 3. (a) P_d ($M_{\rm lim}$) under different $\rm SNR_i$ assumptions and (b) P_d ($M_{\rm lim}$) under different $\rm SNR_c$ assumptions.

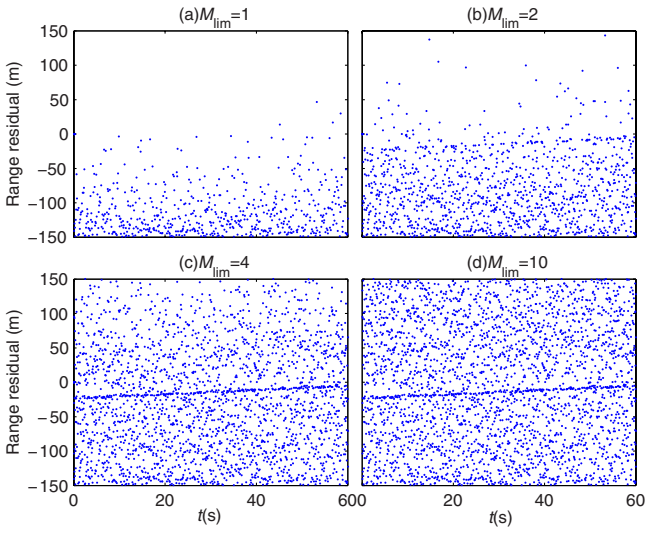

Fig. 4. Range residuals under different $M_{\rm lim}$.

with less data, compared with single-trigger GM-APDs and multi-trigger GM-APDs.

In conclusion, a trigger-controlled GM-APD is introduced. First, the H-LTR method is used to predict the performance of trigger-controlled GM-APDs under different trigger-count upper limits. Based on the H-LTR method, the normalized detection probability is defined to evaluate the detection performance in two typical weak optical signal situations. Theoretical analyses under reasonable assumptions and simplifications prove that through the optimization of the trigger-count upper limit, trigger-controlled GM-APDs can obtain the best detection performance with less data, compared with single-trigger GM-APDs and multi-trigger GM-APDs in impulse noise and continuous noise situations. Finally, the simulation results of the DRLR system using a trigger-controlled GM-APD agrees with the theoretical analysis for the continuous noise situation.

References

1. P. Zhou, C. Liao, Z. Wei, C. Li, and S. Yuan, Chin. Opt. Lett. **9**, 010402 (2011).
2. P. Zhao, Y. Zhang, W. P. Qian, and Y. Xuan, Sci. China Tech. Sci. **58**, 493 (2015).
3. L. Lv, Y. Song, F. Zhu, and X. Zhang, Chin. Opt. Lett. **10**, 040604 (2012).
4. B. Wang, Y. Wang, L. Kong, and A. Wang, Chin. Opt. Lett. **6**, 868 (2008).
5. N. Sangouard, B. Sanguinetti, N. Curtz, N. Gisin, R. Thew, and H. Zbinden, Phys. Rev. Lett. **106**, 120403 (2011).
6. F. Yang, X. Zhang, Y. He, and W. Chen, Chin. Opt. Lett. **12**, 082801 (2014).
7. S. Johnson, P. Gatt, and T. Nichols, Proc. SPIE **5086**, 359 (2003).
8. M. S. Oh, H. J. Kong, T. H. Kim, K. H. Hong, B. W. Kim, and D. J. Park, Rev. Sci. Instrum. **81**, 033109 (2010).
9. D. G. Fouche, Appl. Phys. **42**, 5388 (2003).
10. M. A. Karami, A. Amiri-Sani, and M. H. Ghormishi, Chin. Opt. Lett. **12**, 012501 (2014).
11. P. Zhao, Y. Zhang, Y. M. Hua, and W. P. Qian, Opt. Lett. **40**, 3822 (2015).
12. M. S. Oh, H. J. Kong, and T. H. Kim, Curr. Appl. Phys. **10**, 1041 (2010).
13. G. Kirchner, F. Koidl, F. Friederich, I. Buske, V. Uwe, and R. Wolfgang, Adv. Space Res. **51**, 21 (2013).